



# Ferroptosis of Endothelial Cells Triggered by Erythrophagocytosis Contributes to Thrombogenesis in Uremia

Zhanni Li<sup>1</sup> Meishan Yan<sup>1</sup> Zelong Wang<sup>1</sup> Yao An<sup>1</sup> Xinyu Wei<sup>1</sup> Tingting Li<sup>1</sup> Minghui Xu<sup>1</sup>  
Yanshi Xia<sup>1</sup> Liqiu Wang<sup>2</sup> Chunyan Gao<sup>1</sup>

<sup>1</sup>Department of Medical Laboratory Science and Technology, Harbin Medical University-Daqing, Daqing, China

<sup>2</sup>Department of Clinical Laboratory, The Fifth Hospital, Harbin Medical University, Daqing, China

Address for correspondence: Chunyan Gao, MD, Department of Medical Laboratory Science and Technology, Harbin Medical University-Daqing, Daqing 163000, China (e-mail: gaochunyan1234@163.com).

Thromb Haemost 2023;123:1116–1128.

## Abstract

**Background** Although thrombosis events are the leading complication of uremia, their mechanism is largely unknown. The interaction between endothelial cells (ECs) and red blood cells (RBCs) in uremic solutes and its prothrombotic role need to be investigated.

**Methods and Results** Here, we established an in vitro co-incubation model of uremic RBC and EC as well as a uremic rat model induced by adenine. Using flow cytometry, confocal microscopy, and electron microscopy, we found increased erythrophagocytosis by EC accompanied by increased reactive oxygen species, lipid peroxidation, and impairment of mitochondria, indicating that ECs undergo ferroptosis. Further investigations showed increased proteins' expression of heme oxygenase-1 and ferritin and labile iron pool accumulation in EC, which could be suppressed by deferoxamine (DFO). The ferroptosis-negative regulators glutathione peroxidase 4 and SLC7A11 were decreased in our erythrophagocytosis model and could be enhanced by ferrostatin-1 or DFO. In vivo, we observed that vascular EC phagocytosed RBC and underwent ferroptosis in the kidney of the uremic rat, which could be inhibited by blocking the phagocytic pathway or inhibiting ferroptosis. Next, we found that the high tendency of thrombus formation was accompanied by erythrophagocytosis-induced ferroptosis in vitro and in vivo. Importantly, we further revealed that upregulated TMEM16F expression mediated phosphatidylserine externalization on ferroptotic EC, which contributed to a uremia-associated hypercoagulable state.

**Conclusion** Our results indicate that erythrophagocytosis-triggered ferroptosis followed by phosphatidylserine exposure of EC may play a key role in uremic thrombotic complications, which may be a promising target to prevent thrombogenesis of uremia.

## Keywords

- erythrophagocytosis
- ferroptosis
- endothelial cell
- thrombosis
- uremia

received

September 28, 2022

accepted after revision

June 12, 2023

accepted manuscript online

June 26, 2023

article published online

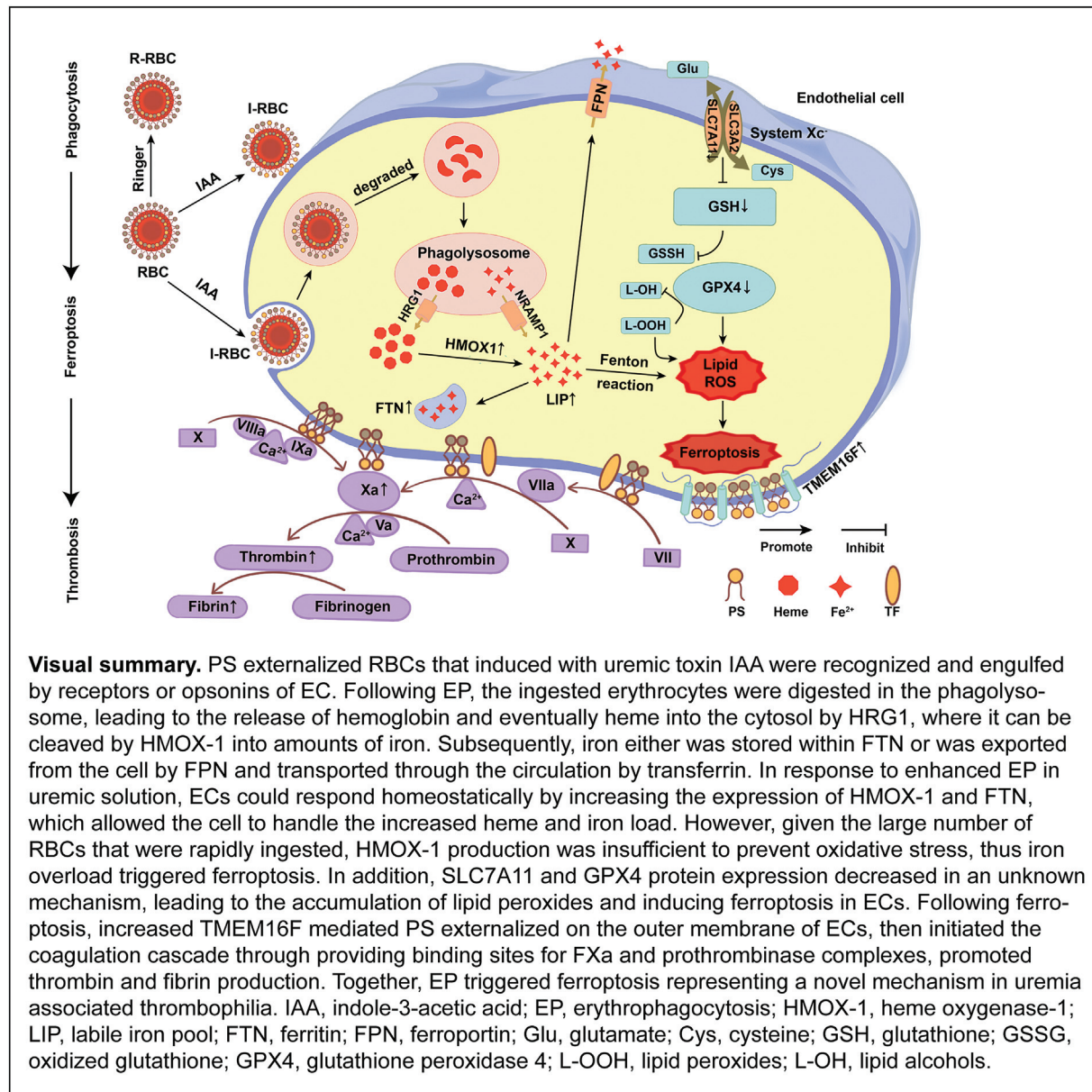
August 3, 2023

DOI <https://doi.org/10.1055/a-2117-7890>  
ISSN 0340-6245.

© 2023. The Author(s).

This is an open access article published by Thieme under the terms of the Creative Commons Attribution-NonDerivative-NonCommercial-License, permitting copying and reproduction so long as the original work is given appropriate credit. Contents may not be used for commercial purposes, or adapted, remixed, transformed or built upon. (<https://creativecommons.org/licenses/by-nc-nd/4.0/>)

Georg Thieme Verlag KG, Rüdigerstraße 14, 70469 Stuttgart, Germany



## Introduction

Uremic patients are at high risk of venous thromboembolism (VTE), stroke, and acute coronary syndrome,<sup>1–3</sup> which may represent the predominant cause of mortality.<sup>4</sup> A better understanding of the pathogenesis of thrombotic tendencies in uremia could help to find novel therapeutic targets to prevent thrombosis in uremia.

Phosphatidylserine, an anionic phospholipid, is usually confined to the inner leaflet of the cell membrane.<sup>5,6</sup> It is externalized to the outer membrane when cell apoptosis is activated. Exposed phosphatidylserine on cells as a critical “eat me” signal for phagocytes provides a catalytic surface for the assembly of tenase and prothrombinase complexes.<sup>7–9</sup> Our previous studies had shown that uremic solutes indoxyl sulfate (IS) and indole-3-acetic acid (IAA) induced eryptosis and enhanced the procoagulant activity of red blood cells

(RBCs) through phosphatidylserine exposure and microparticle release, which contributed to the hypercoagulable state in uremia.<sup>10,11</sup> However, the fate of these phosphatidylserine-exposed RBCs was not investigated. It is well known that macrophages play critical roles in the clearance of senescent RBC and recycling iron in physiological processes, which are called erythrophagocytosis.<sup>12</sup> However, in certain clinical situations such as malaria, immunoglobulin G-mediated hemolytic transfusion reactions, transfusion of storage-damaged RBCs, and uremia, shortened RBC lifespan and increased or pathologic erythrophagocytosis may make professional macrophages overwhelmed, dysfunction, and loss.<sup>13,14</sup> Endothelial cells (ECs) are amateur phagocytes which exist in a large amount on the walls of blood vessels and have the potential phagocytotic ability. Recent studies have reported that ECs have phagocytic properties for lactadherin-opsonized RBC.<sup>15,16</sup> In this study, we found that

injured or eryptotic RBCs by uremic toxins were engulfed by vascular ECs (vECs), and then, we investigated the effects of erythrophagocytosis on ECs.

Ferroptosis is a recently identified iron-dependent cell death characterized by increased iron-dependent reactive oxygen species (ROS) and lipid peroxides, which is morphologically, biochemically, and genetically distinct from apoptosis, necroptosis, and autophagy.<sup>17,18</sup> Ferroptosis plays an important regulatory role in many diseases such as tumors, cardiomyopathy, acute kidney injury, and ischemia/reperfusion.<sup>19–22</sup> However, the role of ferroptosis in the occurrence and development of thrombosis is currently unknown. In this study, we first demonstrated pathologic erythrophagocytosis disrupting the homeostasis of iron metabolism and resulting in iron overload, and subsequently, the increased “free” iron-induced ferroptosis of EC through the Fenton reaction producing multiple ROS and lipid peroxidation products. Following ferroptosis, phosphatidylserine was exposed on EC, which enhanced the procoagulant activity of EC and contributed to the thrombophilic state under the uremic conditions. Our data showed a relationship between erythrophagocytosis, ferroptosis, and thrombogenesis, which further explained coagulation disorders, renal anemia, and inflammation complications in uremic patients.

## Materials and Methods

### Reagents

Detailed description of all reagents can be found in the **►Supplementary Methods** (available in the online version).

### Cells and Animal Model

Peripheral blood was drawn from healthy volunteers and approval from the Ethics Committee of Harbin Medical University according to the Helsinki Declaration was obtained. All animal studies were approved by the Animal Care Committee of Harbin Medical University and conformed to the international guidelines on the ethical use of animals. Detailed information about co-incubation model of uremic RBC and EC in vitro, a uremic rat model induced by adenine, and flow restriction in the inferior vena cava (IVC) is available in the **►Supplementary Methods** (available in the online version).<sup>23–25</sup>

The following were performed as previously described: phagocytosis assay, flow cytometry, electron microscopy, confocal microscopy, HE and MSB staining, Western blot, FXa and prothrombinase assays, thromboelastography testing, malondialdehyde (MDA), glutathione (GSH), catalase (CAT), H<sub>2</sub>O<sub>2</sub>, superoxide dismutase (SOD), and iron quantification assays.<sup>26,27</sup> Detailed information about these methods is available in the **►Supplementary Methods** (available in the online version).

### Statistical Analysis

All values were presented as the mean ± standard deviation. Groups were compared using the two-tailed Student's test or one-way analysis of variance with Tukey's post hoc test. Differences with a *p*-value <0.05 were statistically

significant. Statistical analysis was analyzed by GraphPad Prism 8.0.

## Results

### Phosphatidylserine-Exposed RBCs Were Engulfed, Degraded, and Eliminated by ECs In Vitro

To investigate the increased erythrophagocytosis by ECs in uremic conditions, we set up an in vitro co-incubation model of uremic RBC and cultured EC. Uremic toxin IAA was used to induce phosphatidylserine exposure on RBCs, and ethanol was used as the vehicle because IAA was dissolved by ethanol. Phosphatidylserine exposure was detected through annexin V-FITC binding by confocal microscopy and flow cytometry, respectively. After 24 hours of incubation, compared with RBCs cultured in Ringer solution (R-RBCs), 20 μM IAA-treated RBCs (I-RBCs) had a significantly higher percentage of annexin V binding ( $11.08 \pm 0.44\%$  vs.  $0.15 \pm 0.02\%$ ,  $p < 0.001$ ), and a higher percentage ( $14.03 \pm 1.5\%$ ,  $p < 0.01$ ) in 50 μM IAA (**►Supplementary Fig. S1A**, available in the online version), which is consistent with our previous studies.<sup>9</sup> Confocal microscopy further showed stronger rings of green fluorescence on the outer membrane of I-RBCs compared to R-RBCs (**►Supplementary Fig. S1B, C**, available in the online version). Therefore, in the following co-incubation experiment, we used the RBCs treated with the maximal level of IAA (50 μM) found in uremic patients.<sup>24</sup> Next, we determined the interaction between uremic RBC and EC in the co-incubation model. After co-incubation for 6 hours, images of representative confocal microscopy showed that significantly increased I-RBCs (red) were taken up by ECs (green) compared with R-RBCs (**►Fig. 1A, B**). By flow cytometry, we further quantified the internalization of RBCs by ECs. The percentage of ECs containing RBCs was  $21.47 \pm 1.18\%$  in the I-RBC group, which was significantly higher than that in the R-RBC group ( $1.9 \pm 0.6\%$ ,  $p < 0.001$ ). In addition, I-RBC showed a massively enhanced endocytosis by EC after lactadherin opsonization ( $31.78 \pm 1.27\%$ ,  $p < 0.001$ ), while the extent of phagocytosis was dramatically suppressed when I-RBCs were pretreated with annexin V to block the exposed phosphatidylserine ( $6.83 \pm 1.47\%$ ,  $p < 0.001$ ) (**►Fig. 1C**). We further depicted the dynamic phagocytosis process by scanning electron microscopy (SEM) and transmission electron microscopy (TEM). Representative images of SEM showed that four I-RBCs were trapped, anchored, and endocytosed by EC (**►Fig. 1E**), whereas none of the R-RBC in contact with the EC during 6 hours of co-culture (**►Fig. 1D**). As shown in **►Fig. 1F**, TEM displayed that the EC was extending the pseudopodia and adhering I-RBC, and then I-RBC was captured and internalized by EC (**►Fig. 1G**). After 12 hours of co-incubation, erythrocytes were digested and degraded into fragments in EC (**►Fig. 1H**). Within 24 hours, nearly all phagocytic intracellular RBCs had disappeared, leaving only their membrane ruffles or empty vesicles (**►Fig. 1I, J**), suggesting that degradation was virtually complete. Taken together, these results indicated that uremic RBCs were indeed endocytosed by ECs and in a phosphatidylserine-dependent manner.



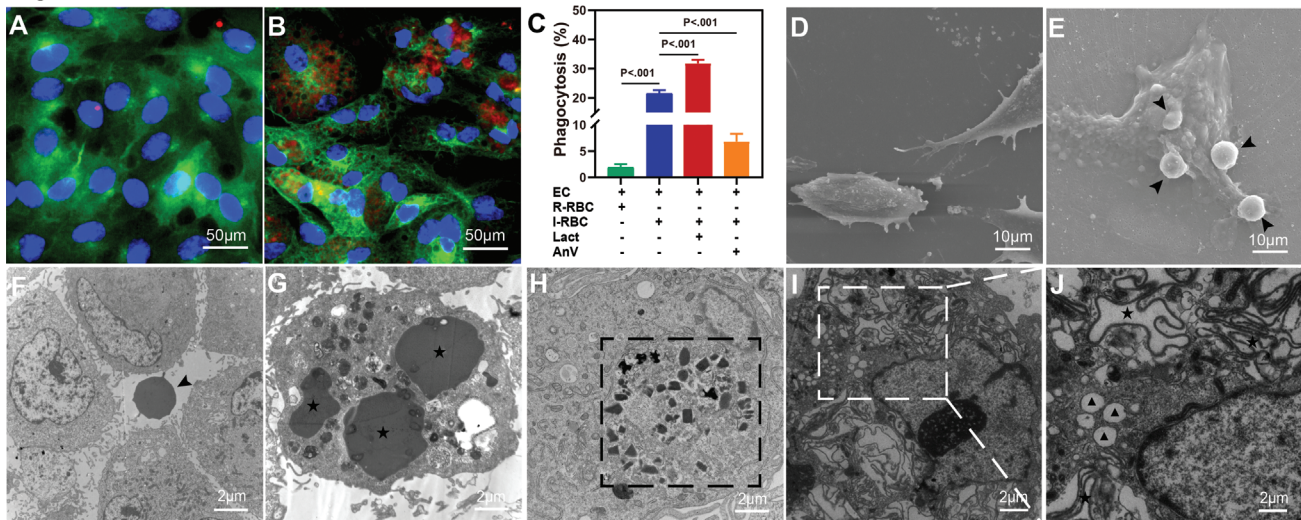


**Fig. 1** Phosphatidylserine exposed RBCs were engulfed, degraded, and eliminated by ECs in vitro. ECs were incubated with R-RBCs and I-RBCs for 6 hours, respectively. After washing and removing the nonadherent or nonphagocytosed RBCs, immunofluorescence staining was applied to definitively determine the phagocytosis of RBCs by ECs. RBCs were stained with CD235a (red). The cytoskeleton and nuclei of ECs were labelled with tubulin (green) and Hoechst 33342 (blue), respectively. R-RBCs (A) and I-RBCs (B) were taken up or engulfed by ECs. (C) RBCs were stained with 1  $\mu$ M CMFDA (green) for 30 minutes at room temperature, and then cocultured with ECs for 6 hours in the presence or absence of 2 nM Lact or 2 nM AnV. The phagocytic percentage was counted by flow cytometry. All data were representative of at least three independent experiments and values were expressed as mean  $\pm$  SD. Scanning electron microscopy examination of adhered RBCs to the surface of ECs after 6 hours of incubation, several I-RBCs (arrow) were trapped, anchored, and internalizing by EC (E), whereas none of the R-RBC adhered to EC (D). Transmission electron microscopy images displayed a kinetic process that I-RBCs were engulfed and degraded in ECs for 24 hours. I-RBC (arrow) was extending the pseudopodia and adhering to EC (F), and then RBCs (stars) were internalized in EC after 6 hours of coculture (G). (H) After 12 hours of co-incubation, erythrocytes were digested and degraded into fragments in EC (dotted box). (I) After 24 hours, nearly all phagocytosed intracellular RBCs had disappeared, leaving only their membranes. (J) Local magnification of RBC membrane ruffles (star) and empty vesicles (triangle) in EC. AnV, annexin V; EC, endothelial cell; IAA, indole-3-acetic acid; I-RBC, RBCs cultured in Ringer solution with 50  $\mu$ M IAA; Lact, lactadherin; R-RBC, RBCs cultured in Ringer solution; SD, standard deviation.

### ECs Underwent Ferroptosis following Enhanced Erythrophagocytosis

The distinction between ferroptosis and other forms of cell death is the dramatic morphological changes of mitochondria in ferroptosis. When observing the ultrastructure of ECs through TEM, compared with the normal mitochondria in ECs without erythrophagocytosis ( $\rightarrow$  Fig. 2A), we found detailed impairments of mitochondria, including content lost, cristae reduced or disappeared ( $\rightarrow$  Fig. 2B, C), increased membrane density, condensed cristae ( $\rightarrow$  Fig. 2D), and enhanced Fiameng score (a semiquantitative evaluation method of the mitochondrial ultrastructure) in I-RBC-treated ECs ( $\rightarrow$  Fig. 2E). To further verify that increased erythrophagocytosis-induced ferroptosis in ECs, cell viability, ROS, and lipid peroxidation were detected, respectively. We found that erythrophagocytosis led to significantly decreased viability of ECs, which could be rescued by ferrostatin-1 (Fer-1) and deferoxamine (DFO), respectively ( $\rightarrow$  Fig. 2F). In addition, compared to R-RBC-treated EC, there were significantly increased DCF and C11-Bodipy fluorescence in I-RBC-treated EC after 12 hours of incubation, which were effectively reduced by treatment with Fer-1 or DFO ( $\rightarrow$  Fig. 2G, H). These results further indicated that increased erythrophagocytosis led to EC ferroptosis.

### Erythrophagocytosis-Induced Ferroptosis of ECs via Iron Overload and Amino Acid Metabolism Disorder

Although increasing evidence suggests that ECs experience ferroptosis following phagocytosis of uremic RBCs, the un-

derlying mechanism is poorly understood. In human, approximately 80% of heme is present in erythrocytes, and we speculated that iron overload may play an important role in erythrophagocytosis-induced EC ferroptosis. Therefore, the proteins that regulated intracellular iron homeostasis were detected. As we expected, there was significantly higher iron content in ECs that co-incubated with I-RBCs than that with R-RBCs, whereas the intracellular active iron was decreased in I-RBC-treated ECs with the addition of DFO to chelate iron, but it was similar between the two groups when pretreated with Fer-1 ( $\rightarrow$  Fig. 3A). The level of heme oxygenase-1 (HO-1) protein expression was significantly increased in I-RBC-treated ECs. Moreover, neither Fer-1 nor DFO could inhibit the upregulated HO-1 ( $\rightarrow$  Fig. 3B). Consistent with the increased HO-1 levels, we also found increased ferritin (FTN) protein levels in the I-RBC-treated ECs, while the expression of FPN responsible for iron efflux did not change. Furthermore, when I-RBC-treated ECs were incubated with DFO, FTN significantly decreased, but there was no difference when pretreated with Fer-1 ( $\rightarrow$  Fig. 3C, D), suggesting iron overload played a critical role in the ferroptosis of EC triggered by erythrophagocytosis. By Western blot assay, we found that in addition to iron overload, I-RBC-treated ECs had decreased levels of glutathione peroxidase 4 (GPX4) and SLC7A11 compared with R-RBC-treated ECs. Moreover, both of the two proteins rescued significantly following the administration of Fer-1 and DFO ( $\rightarrow$  Fig. 3E, F), indicating amino acid metabolism disorder also occurred in erythrophagocytosis-



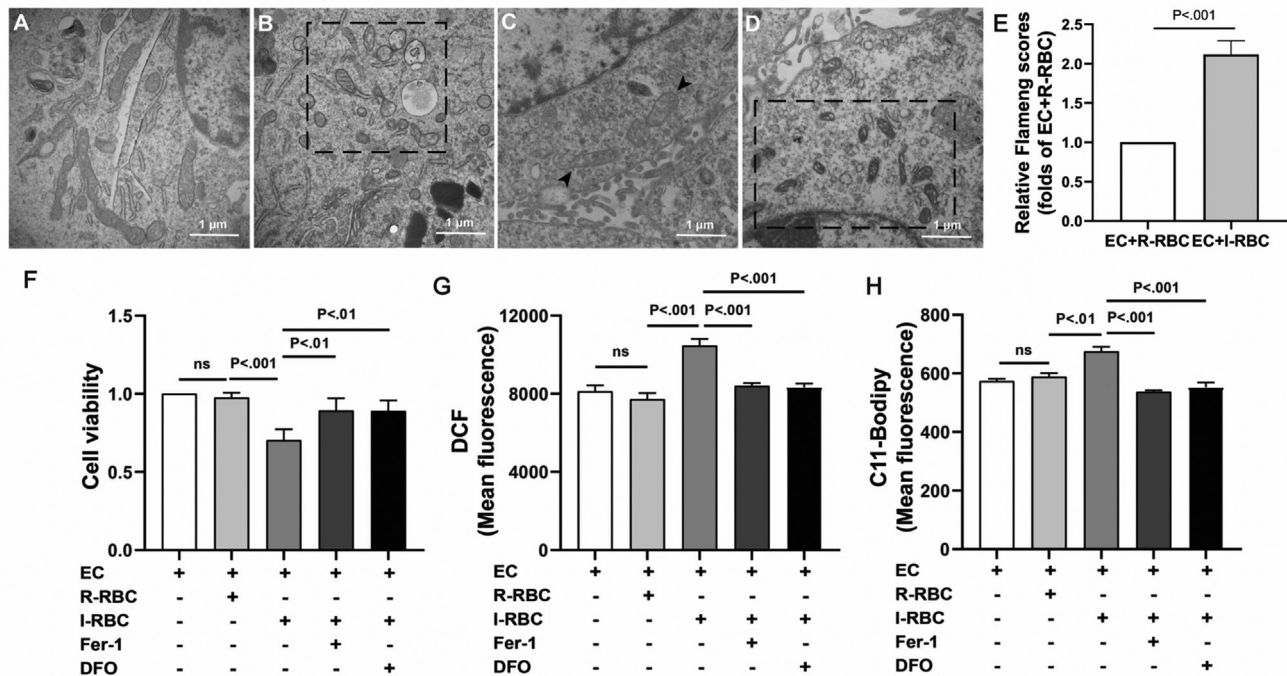


**Fig. 2** ECs undergo ferroptosis following enhanced erythrophagocytosis. The ultrastructure of mitochondria in ECs was analyzed by transmission electron microscopy in the erythrophagocytosis model. (A) Normal mitochondria in EC without erythrophagocytosis. In our erythrophagocytosis model, ECs cocultured with I-RBCs exhibit morphological changes of mitochondria around the internalized RBC fragments including mitochondrial integrity impaired, content lost, cristae reduced (dotted box) (B) and disappeared (C), membrane density increased, and cristae condensed (D). ECs were incubated with each group of RBCs for 12 hours with or without 5  $\mu$ M Fer-1 or 200  $\mu$ M DFO. (E) The Flaming scores were used to evaluate the mitochondrial ultrastructure. (F) The viability of ECs was assessed by the CCK-8 test. Each group of cells was incubated with DCFH-DA or C11-BODIPY for 30 minutes at 37°C; after washing, the levels of ROS (G) and lipid peroxidation (H) in ECs were determined by flow cytometry. All data were representative of at least three independent experiments and values were expressed as mean  $\pm$  SD. DFO, deferoxamine; EC, endothelial cell; Fer-1, ferrostatin-1; IAA, indole-3-acetic acid; I-RBC, RBCs cultured in Ringer solution with 50  $\mu$ M IAA; R-RBC, RBCs cultured in Ringer solution; ROS, reactive oxygen species; SD, standard deviation.

triggered ferroptosis by suppressing the expression of system  $X_c^-$  and led to a reduced generation of GPX4.

### Ferroptosis Followed by Erythrophagocytosis Enhanced the Procoagulant Activity of ECs

Since ECs experienced ferroptosis after the uptake of large numbers of RBCs, we considered that this could disrupt the clotting balance of ECs. To explore whether ferroptosis enhance the procoagulant activity of ECs, we examined the procoagulant activity of ECs by one-stage recalcification time assay. As shown in ►Fig. 4A, after 12 hours of incubation, the coagulation time of ECs cultured with I-RBCs was  $151.22 \pm 10.29$  seconds, which significantly reduced when compared with ECs cultured with R-RBCs ( $197.07 \pm 8.36$  seconds,  $p < 0.001$ ). To understand the role of phosphatidylserine exposure in ferroptosis-induced procoagulant activity of EC, coagulation inhibition assays were further performed on EC. The procoagulant activity of ECs was inhibited over 90% by 128 nM lactadherin. It is well known that one of the important roles of phosphatidylserine is a catalytic surface for the assembly of FXa and prothrombinase complexes. We further investigated the capacity of EC to support intrinsic, extrinsic FXa, and thrombin that contribute to the procoagulant activity. As shown in ►Fig. 4B, I-RBC-treated ECs significantly increased the production of the three procoagulant enzyme complexes compared with R-RBC-treated ECs,

which were inhibited by 128 nM lactadherin up to 90%. Results from inhibition assays further confirmed that phosphatidylserine played a crucial role in the procoagulant activity of ECs undergoing ferroptosis. More recent studies have shown that TMEM16F served as phospholipid scramblase and was upregulated in ferroptosis. Therefore, we also evaluated the expression and role of TMEM16F in the erythrophagocytosis-induced ferroptosis. We found that I-RBC-treated ECs exhibited significantly higher TMEM16F expression and phosphatidylserine exposure compared to ECs with or without cocultured R-RBCs by Western blotting and flow cytometry, respectively (►Fig. 4C, D). In addition, confocal microscopy visually demonstrated that TMEM16F expression (green) and phosphatidylserine exposure (green) increased significantly in the I-RBC-treated ECs compared with the R-RBC-treated ECs (►Fig. 4E-J).

### Erythrophagocytosis and Ferroptosis Occurred in the Kidney of Uremic Rats

To better understand the mechanisms of thromboembolic disorders in uremia, we established an adenine-induced animal model of chronic kidney disease. Consistent with previous reports,<sup>27</sup> 0.75% adenine treatment for 4 weeks was effective in causing chronic kidney disease in rats. As shown in ►Supplementary Table S1 (available in the online version), adenine-treated rats significantly decreased the body

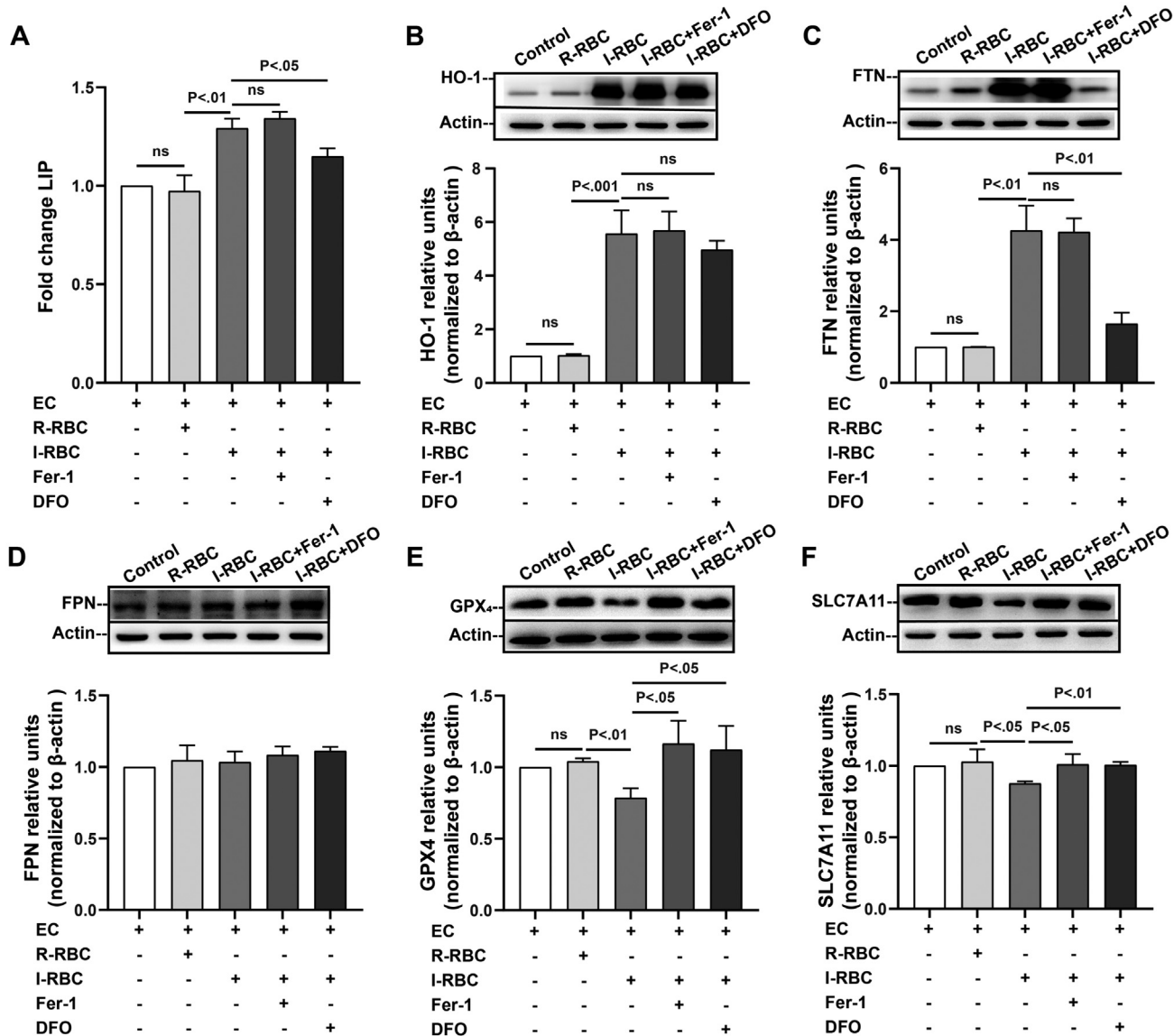


**Fig. 3** Iron overload and amino acid metabolism contributed to erythrophagocytosis-induced ferroptosis of ECs. ECs were incubated with R-RBC and I-RBC with or without 5  $\mu$ M Fer-1 (I-RBC + Fer-1 group) or 200  $\mu$ M DFO (I-RBC + DFO group) for 12 hours, respectively. (A) Calcein fluorescence assays. ECs were stained with calcein-AM (1  $\mu$ M) and fluorescence intensity was measured by flow cytometry. The results were expressed as the mean fold changes versus untreated ECs (mean  $\pm$  SD,  $n$  = 3 experiments). (B–F) Protein levels of HO-1, FTN, FPN, GPX4, and SLC7A11 in ECs were detected by Western blotting. The relative density of the protein bands was quantified and normalized to  $\beta$ -actin (mean  $\pm$  SD,  $n$  = 3 experiments). DFO, deferrioxamine; EC, endothelial cell; Fer-1, ferrostatin-1; FPN, ferroportin; FTN, ferritin; GPX4, glutathione peroxidase 4; HO-1, heme oxygenase-1; IAA, indole-3-acetic acid; I-RBC, RBCs cultured in Ringer solution with 50  $\mu$ M IAA; LIP, labile iron pool; R-RBC, RBCs cultured in Ringer solution; SD, standard deviation.

weight, RBC, and hemoglobin, and significantly increased plasma urea, creatinine, uric acid, and phosphorus compared with control rats, which are in line with the characteristics of uremia. Likewise, compared with control rats, representative images of HE staining from kidney of the adenine-treated rats showed the characteristic structural changes including glomerular injury, tubulointerstitial fibrosis, interstitial inflammatory infiltrates, tubular distend, and vacuolar degeneration of epithelial cells (**Supplementary Fig. S2A, B**, available in the online version). Histological analysis of kidney sections showed that the number, diameter, and surface area of the glomerulus were markedly reduced in the adenine-treated group compared to the control group.

Compared with the control group, the renal coefficient (the ratio of the left kidney's weight to its body weight) was significantly higher in the adenine-treated group (**Supplementary Fig. S2C–F**, available in the online version). These results indicated adenine administration effectively induced uremia in rats. Then, we further explored the association and underlying mechanisms of erythrophagocytosis, ferroptosis, and thrombogenesis in our uremic rat model. Representative light microscopy images of a blood vessel in the kidney showed that multiple erythrocytes were adhered to the vascular wall and internalized in vEC (**Fig. 5A**) and accompanied by microthrombosis in the microvasculature of the uremic kidney by MSB staining

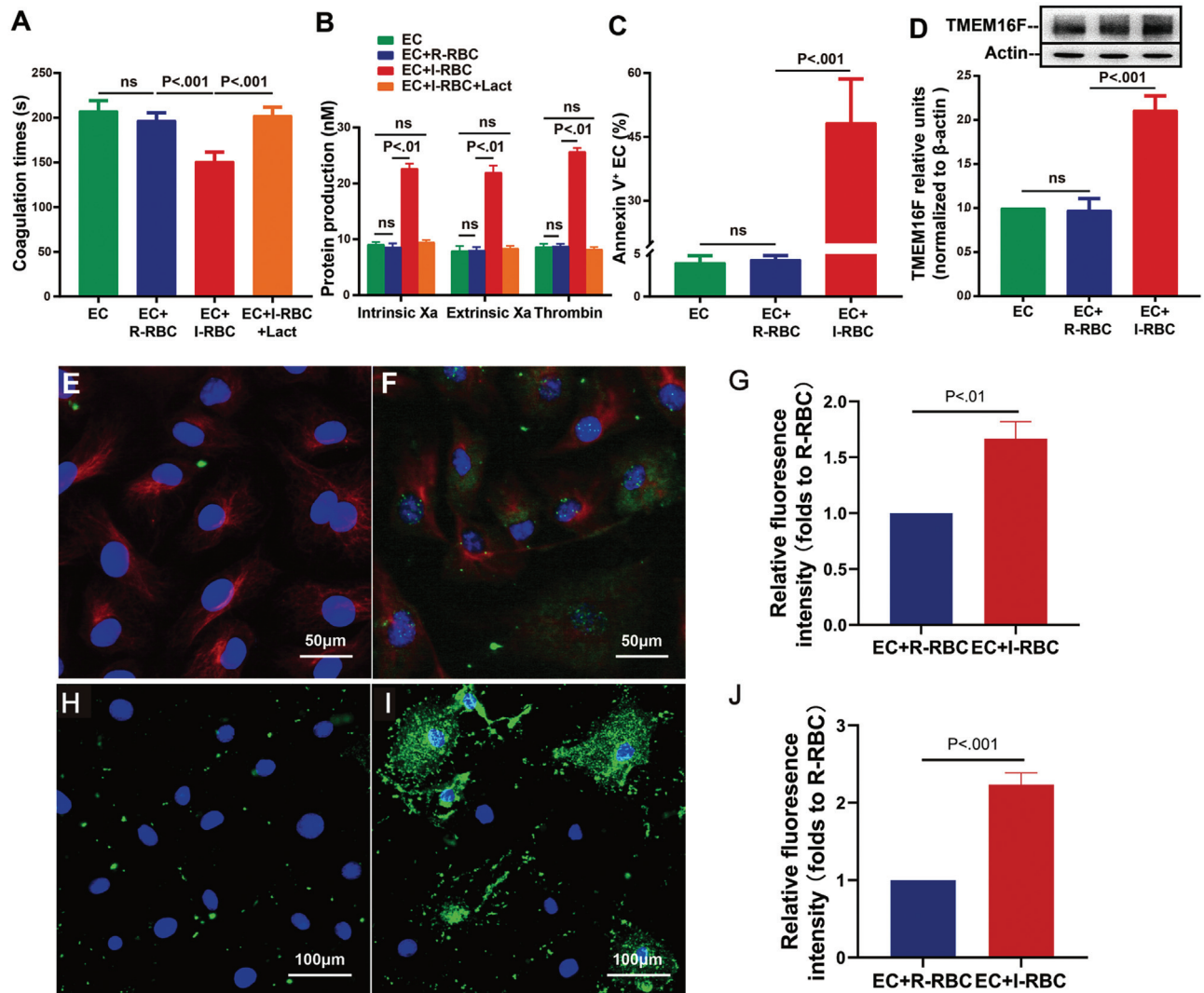


**Fig. 4** Ferroptosis followed by erythrophagocytosis enhanced the procoagulant activity of ECs. ECs were cocultured with R-RBC and I-RBC for 12 hours, respectively. After washing and removing the nonadherent or nonphagocytosed RBCs, ECs were collected for the one-stage recalcification time assay. (A) In the absence or presence of 128 nM Lact, coagulation times of 100  $\mu$ L ECs ( $10^3$ ) in each group were shown. Results were displayed as mean  $\pm$  SD for at least three independent experiments. (B) Formation and inhibition assays of procoagulant enzyme complexes. FXa and thrombin production of ECs ( $10^3$ ) were shown. Intrinsic FXa formation was measured in the presence of FIXa, FVIII, and thrombin. Extrinsic FXa production was assessed in the presence of FVIIa. Thrombin generation was investigated in the presence of FXa and FVa. The capacity of 128 nM Lact was evaluated to block procoagulant enzyme complexes on ECs. Data are mean  $\pm$  SD. (C) ECs were collected and incubated with annexin V- FITC for 30 minutes in the dark, and then flow cytometry analyzed the phosphatidylserine exposure of ECs. Results were expressed as mean  $\pm$  SD. (D) The expression level of TMEM16F in ECs was detected by Western blotting. The relative density of the protein bands was quantified and normalized to  $\beta$ -actin (mean  $\pm$  SD,  $n = 3$ ). Expression of TMEM16F (green) in ECs was determined by immunofluorescence staining. The cytoskeleton and nuclei of ECs were labeled with tubulin (red) and Hoechst 33342 (blue), respectively. (E) No TMEM16F staining was found in the R-RBC-treated ECs. (F) Much green fluorescence was visible on ECs after coculturing with I-RBC. (G) The relative fluorescence intensity of TMEM16F. Confocal microscopy images of phosphatidylserine (green) externalized to the outer membrane of ECs co-incubated with I-RBC (I) or R-RBC (H). (J) The relative fluorescence intensity of phosphatidylserine. EC, endothelial cell; IAA, indole-3-acetic acid; I-RBC, RBCs cultured in Ringer solution with 50  $\mu$ M IAA; Lact, lactadherin; R-RBC, RBCs cultured in Ringer solution; SD, standard deviation.

(**Fig. 5B**). More importantly, we also examined the interaction between RBC and EC inside the blood vessel by TEM. Representative images showed that the erythrocyte was trapped and anchored by the EC in the vessel of kidney (**Fig. 5C**), and several erythrocytes were endocytosed and degraded to some fragments by the EC (**Fig. 5D**). Similarly to that observed in vitro, we found morphological changes of the mitochondria in the EC, such as cristae reduced and content lost (**Fig. 5E**).

Then, iron metabolism and lipid peroxidation signaling were detected in kidney tissue. Representative images of Perls blue plus diaminobenzidine staining revealed increased reactive iron deposits on the microvasculature EC in the uremic kidney compared to control, which further proved that iron overload was the most important mechanism in erythrophagocytosis-triggered EC ferroptosis (**Fig. 5F-I**). Moreover, compared with the control group, the uremic rats had significantly higher content of iron, MDA,



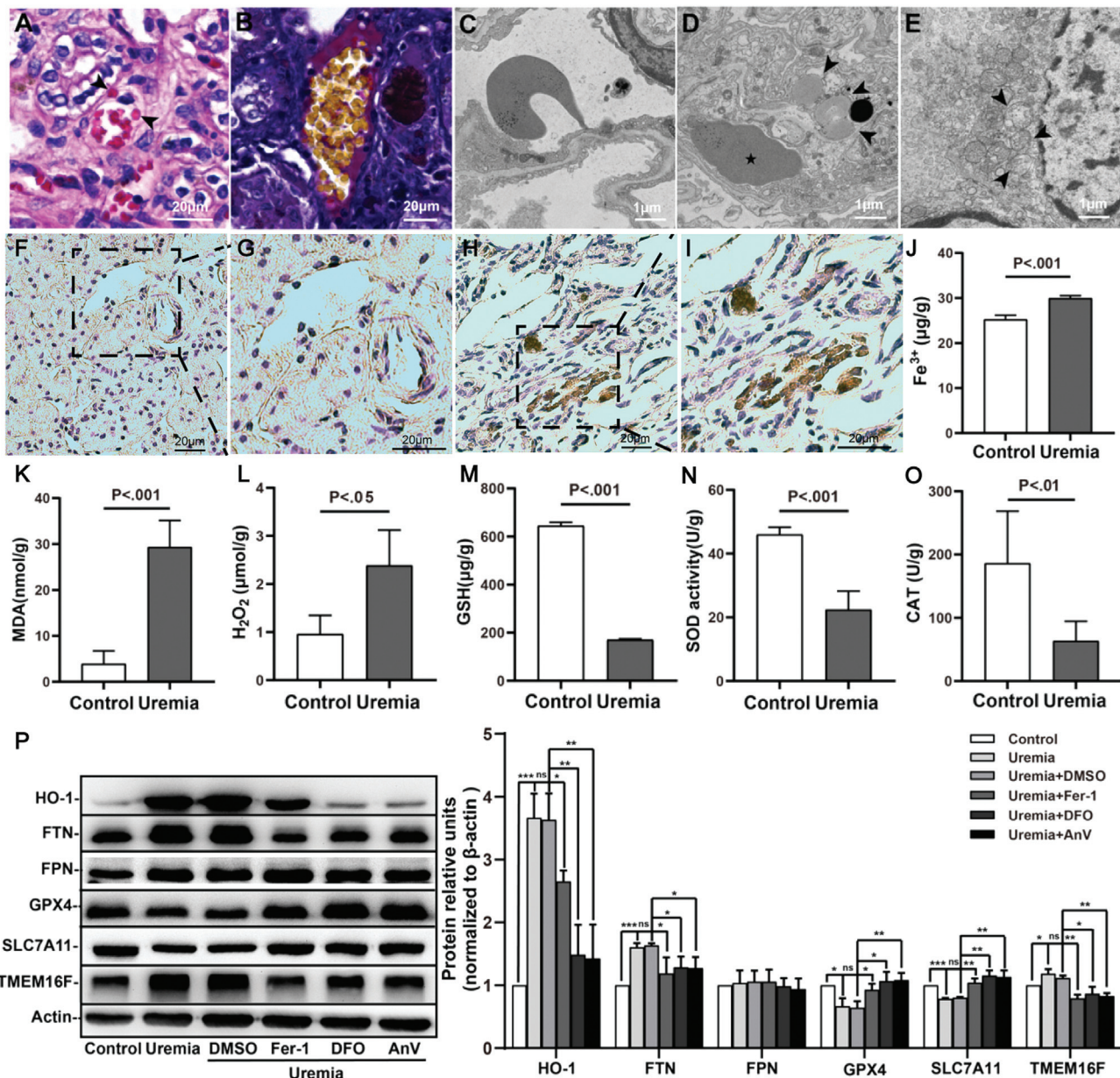


**Fig. 5** Erythrophagocytosis triggered ferroptosis of kidney in the uremic rats. Histological analyses of the kidney tissue section in three different stainings (HE, MSB, and DAB-enhanced Prussian blue). (A) Light microscopy image of a blood vessel showed internalization of multiple RBCs by ECs (indicated by arrow). (B) Representative image of MSB staining showed RBC aggregates and fibrin on the microvasculature EC surface in the uremic kidney. (C) Transmission electron microscopy image of an erythrocyte trapped and anchored by EC in the vessel of the uremic kidney. (D) Several erythrocytes were endocytosed (star) and degraded to some fragments (arrow) by ECs. (E) The mitochondrial ultrastructure of renal vascular ECs from uremic rats showed cristae reduced and content lost (arrow). (F–I) Kidney sections were stained with DAB-enhanced Prussian blue to detect iron deposits on the microvasculature EC. Representative images of kidney sections from the uremia group (F and G) and control (H and I) are shown. Panels (G) and (I) show the magnified images of selected areas from (F) and (H), respectively. (J–O) Adenine-induced ferroptosis in the kidney of rats. (J) The iron content of the kidney tissue was measured in each group. (K) The level of lipid peroxide MDA in each group. (L) The level of H<sub>2</sub>O<sub>2</sub> in each group. (M) The GSH level in each group. (N) The activity of SOD in each group. (O) The activity of CAT in each group. All data are mean ± SD of at least three independent experiments (n = 5 rats/group). (P) Western blotting of HO-1, FTN, FPN, GPX4, SLC7A11, and TMEM16F protein expression of kidney tissue in control and uremic rats treated with or without 1% DMSO, 1 mg/kg Fer-1, 25 mg/kg DFO, and 0.2 mg/kg AnV, respectively (n = 5 rats/group). Data are expressed as the mean ± SD of at least three independent experiments. The relative density of protein bands was quantified and normalized to β-actin. AnV, annexin V; CAT, catalase; DFO, deferoxamine; EC, endothelial cell; Fer-1, Ferrostatin-1; FPN, ferroportin; FTN, ferritin; GPX4, glutathione peroxidase 4; GSH, glutathione; H<sub>2</sub>O<sub>2</sub>, hydrogen peroxide; HE, hematoxylin-eosin; HO-1, heme oxygenase-1; MDA, malondialdehyde; MSB, Martius Scarlet Blue; SD, standard deviation; SOD, superoxide dismutase.

and H<sub>2</sub>O<sub>2</sub>, as well as decreased GSH content, SOD, and CAT activity, all of which are also characteristic markers of ferroptosis and indicate enhanced oxidative stress in the adenine-induced uremic rat model (►Fig. 5J–O). To further confirm the occurrence of ferroptosis following increased erythrophagocytosis *in vivo*, adenine-treated rats were simultaneously treated with annexin V to block the phagocytosis pathway, Fer-1 to inhibit ferroptosis, and DFO to chelate iron, respectively. Next, we found that compared with the control group, the protein expression of HO-1, responsible for heme breakdown, was significantly increased in uremic kidney tissue. Consistent with increased HO-1 and iron, FTN responsible for storing excess iron also increased in the uremic group. Both proteins were inhibited by Fer-1, DFO, and annexin V, respectively. However, FPN, the only iron efflux channel located on the surface of the cell membrane, was no different between the two groups. Additionally, the expression levels of ferroptosis characteristic proteins GPX4 and SLC7A11 in uremic renal were significantly lower than those in the corresponding control group and could be reversed by Fer-1, DFO, and annexin V, which revealed that in addition to iron metabolism, amino acid metabolism also involved in erythrophagocytosis-triggered ferroptosis in our uremic model. We also detected the protein expression of TMEM16F that serves as a phospholipid scramblase, consistent with the results *in vitro*, and TMEM16F increased in the renal tissue of the adenine-treated rats but reduced in uremic rats treated with Fer-1, DFO, and annexin V compared to the control group (i.e., nontreated) (►Fig. 5P). These series of results confirmed that erythrophagocytosis-induced ferroptosis indeed occurred *in vivo*, and both iron overload and lipid peroxidation contributed to the pathological process.

### Erythrophagocytosis-Induced Ferroptosis of ECs Promoted Hypercoagulability in Uremic Rats

To confirm whether erythrophagocytosis-induced ferroptosis plays a role in uremia-associated thrombogenesis, a flow restriction model was used. In response to the restriction of venous blood flow, all (4 of 4) uremic rats developed a thrombus within 6 hours after flow stasis in the IVC. And four control rats also formed a visible thrombus after 6 hours of stasis (►Fig. 6A). Moreover, weight, length, and the index of weight (mg)/length (mm) of the thrombus in uremic group were all significantly higher than in the control group, suggesting the thrombus was tighter and denser in uremic rats. However, treating adenine-fed rats with Fer-1, DFO, or annexin V significantly reduced the parameters of thrombus (►Fig. 6B–D). Next, the phosphatidylserine exposure of erythrocytes was analyzed by flow cytometry and, as expected, the percentage of annexin V-positive erythrocytes significantly increased in uremic rats ( $5.97 \pm 0.49\%$ ) compared to healthy controls ( $1.22 \pm 0.08\%$ ,  $p < 0.001$ ) (►Fig. 6E). Thromboelastography was used in our study to further monitor dynamic real-time pictures of coagulation in rats. There was a significant difference between uremic rats and control rats, with uremic rats having a shorter R time, and larger  $\alpha$  angle, maximum amplitude (MA), and clotting index (CI). Not surprisingly, with the addition of Fer-1, DFO, and

annexin V in uremic rats, the R time was markedly prolonged, while  $\alpha$  angle, MA, and CI were reduced compared to rats only treated with adenine (►Fig. 6F–J), which further proved the contribution of ferroptosis in blood hypercoagulability of uremic rats. Taken together, these results confirmed that erythrophagocytosis-induced EC ferroptosis accompanying phosphatidylserine exposure led to a prothrombotic state and local thrombus formation (Visual Summary).

## Discussion

Uremia might be at high risk of cardiovascular and thrombotic events that require special attention.<sup>28</sup> A better understanding of the prothrombotic mechanisms of uremic toxins could help to find novel therapeutic targets to prevent thrombosis in uremia. In this study, to investigate the role of uremic toxin exposure on RBC and its effect on EC function, we set up an *in vitro* co-incubation model of uremic RBC and EC that may mimic uremic condition and an adenine-induced chronic kidney disease rat model. We first found that uremic solute IAA-treated phosphatidylserine-exposed erythrocytes were sequestered, endocytosed, and degraded by EC *in vitro*. Then, increased erythrophagocytosis triggered EC ferroptosis and induced a procoagulant phenotype on EC through increased phosphatidylserine exposure that is mediated by TMEM16F. Furthermore, thromboelastography and IVC ligation-induced flow stasis model confirmed that uremic rats exhibited the hypercoagulable state and were more prone to develop VTE, which was related to erythrophagocytosis-induced ferroptosis. More importantly, we demonstrated that iron overload and perturbations of amino acid metabolism were the most important mechanism of erythrophagocytosis-triggered EC ferroptosis.

It is well known that the ageing RBCs are mainly cleared by macrophage, named erythrophagocytosis.<sup>29</sup> Professional phagocytes such as macrophages and dendritic cells are the main phagocytes, which have the capacity to remove dead cells and other foreign materials in the body.<sup>30</sup> However, professional macrophages may become overwhelmed by the excessive amounts of eryptotic or damaged RBCs in uremia, the amateur phagocytes which can also participate in efferocytosis when needed. Amateur phagocytes are nonmyeloid progenitor/nonimmune cells that include differentiated cells (e.g., epithelial cells, fibroblasts, and ECs) and stem cells.<sup>31</sup> ECs as amateur phagocytes which exist in a large amount on the walls of blood vessels represent the first barrier in contact with erythrocytes and have the potential phagocytotic ability.<sup>32</sup> Ageing or damaged RBCs express phosphatidylserine on their surface which can directly bind to Stabilin-2 or Tim-4 on the macrophage or via opsonins such as Gas-6, lactadherin, or thrombospondin-1.<sup>33</sup> The ability of uremic plasma to promote erythrophagocytosis may be associated with the proinflammatory state, enhanced oxidative stress, and the accumulation of toxins.<sup>34,35</sup> Moreover, increased erythrophagocytosis could accompany by decreased levels of CD47, a do not eat me signal.<sup>36</sup> Our previous studies demonstrated that ECs could endocytose activated platelets, apoptotic neutrophils, and acute promyelocytic leukemia

cells.<sup>24,37,38</sup> Catan et al reported that vECs were able to bind and internalize aged/glycated RBC in diabetic conditions and may promote vulnerable atherothrombotic plaques to rupture.<sup>39</sup> However, the effects on ECs' biology of progressively ingesting large numbers of RBCs are not completely understood; moreover, the relationship between erythrophagocytosis and procoagulant activity of ECs in uremia has not been explored. In our RBC treatment model, we found that ECs engulfed large amounts of phosphatidylserine-exposed IAA-induced erythrocytes even with no bridge molecules, and exhibited morphologic abnormal mitochondria, increased ROS and lipid peroxidation, all of which were all reduced by treatment with Fer-1 or DFO, indicating ECs undergo ferroptosis following enhanced erythrophagocytosis in the uremic environment. Our previous studies have reported that uremic toxins such as uric acid, IAA, and IS could significantly increase phosphatidylserine exposure of RBCs.<sup>11,40</sup> In the present study, we chose one of the uremic toxins IAA, and we

suggested that other uremic toxins including urea, creatinine, oxalic acid, uric acid, and IS also play a similar role in erythrophagocytosis-triggered ferroptosis of EC and followed procoagulant activity. The effect of other toxins on this process will be detected in the future.

We then sought to explore the mechanisms of erythrophagocytosis-induced ferroptosis in EC. As a complex form of cell death, ferroptosis mainly involves three biochemical metabolisms, including iron, amino acid, and lipid metabolism.<sup>41</sup> We hypothesized iron disorder may be the most important reason because plenty of hemoglobin was degraded in the EC after phagocytosis of RBCs. Usually, macrophages play important physiological roles in iron metabolism and recycling by increasing the expression of HO-1 and FTN to handle the increased heme and iron load, thus keeping homeostatically and protecting it from severe oxidative stress.<sup>42</sup> However, the biological role of iron metabolism in

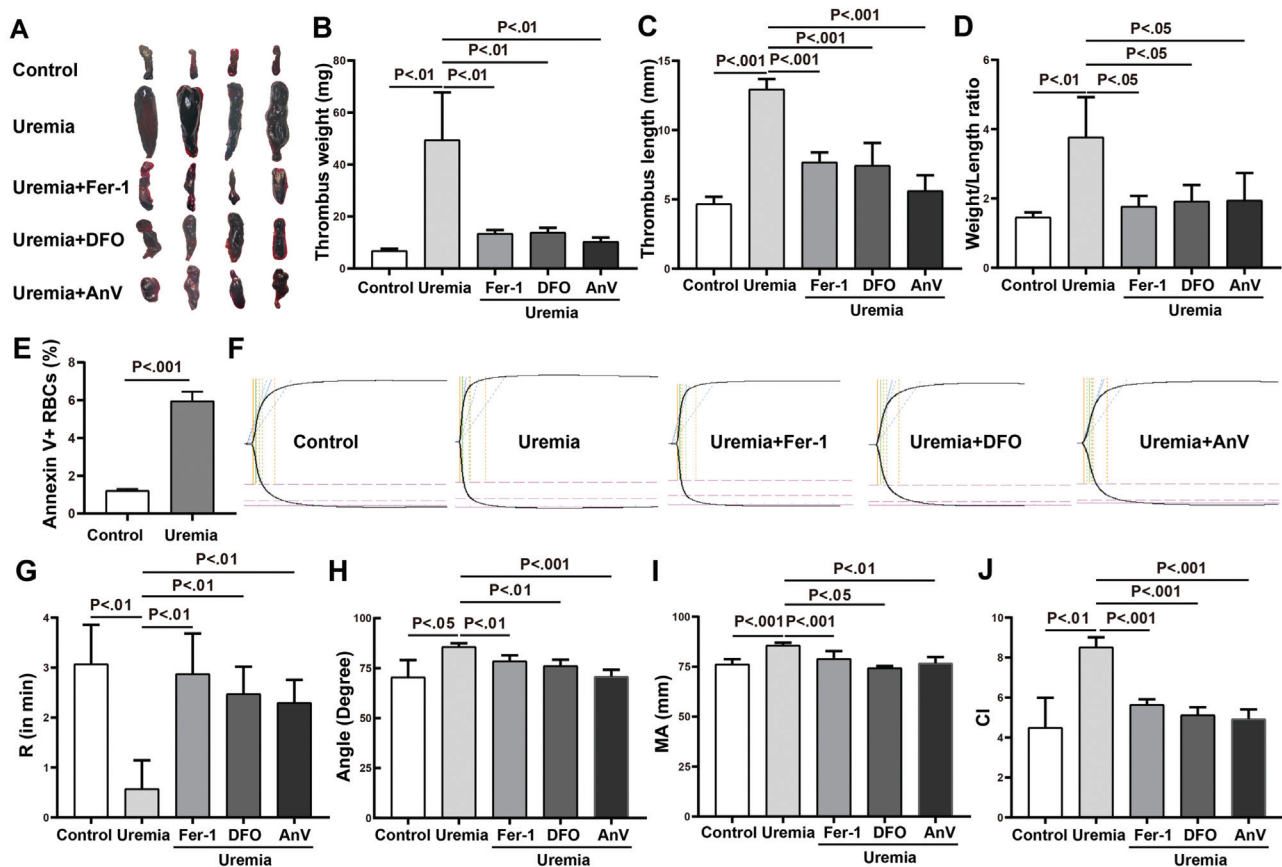


**Fig. 6** Erythrophagocytosis-induced ferroptosis contributed to hypercoagulability in uremic rats. IVC was ligated to obtain complete blood stasis in rats. After 6 hours of flow restriction, rats ( $n = 4$  per group) were euthanized and the IVC-containing thrombi were harvested. (A) Representative images of thrombus from control and uremic rats treated with or without Fer-1, DFO, and AnV. The weight (B), length (C), and weight/length ratio (D) of the thrombus in each group of rats are shown. (E) RBCs from control and uremic rats were stained with annexin V-FITC and analyzed by flow cytometry. Data were expressed as the mean  $\pm$  SD of four independent experiments. The entire hemostatic system was monitored by thromboelastography. An amount of 1 mL of citrated whole blood was drawn (blood:citrate [sodium citrate 3.8%]; 8:2) from each group of rats ( $n = 4$ ) via cardiac puncture and mixed with 40  $\mu$ L kaolin. 340  $\mu$ L citrated blood was mixed with 20  $\mu$ L  $\text{CaCl}_2$  (0.2 M) for thromboelastography analysis. (F) Various representative thromboelastography traces showed a real-time and dynamic picture of coagulation in each group. Major coagulation parameters were analyzed including R time (G),  $\alpha$  angle (H), MA (I), and CI (J). Results were mean  $\pm$  SD ( $n = 4$  rats/group).  $\alpha$  angle, alpha angle; AnV, annexin V; CI, clotting index; DFO, deferoxamine; Fer-1, ferrostatin-1; IVC, inferior vena cava; MA, maximum amplitude; R time, reaction time; SD, standard deviation.



erythrophagocytosis-induced EC ferroptosis remains poorly understood. In the present study, we systematically studied the protein expression in the pathway of iron metabolism of ECs following clearance of RBCs. We found an increased accumulation of free iron and FTN in EC incubated with I-RBCs, while the FPN responsible for iron efflux was no different. Moreover, treatment of ECs with Fer-1 did not decrease the LIP and the content of FTN, whereas they were both reduced after treatment with the iron chelator DFO. Therefore, we speculated that iron overload in ECs eventually leads to ferroptosis. We further investigated several molecules in iron and redox metabolism that have been implicated in ferroptosis. Although HO-1 was thought to be a protective antioxidant enzyme, growing data suggest it plays a positive role in ferroptosis.<sup>43</sup> Recent studies have demonstrated that HO-1 drives ferroptosis by promoting iron overload in cardiomyopathy, hemochromatosis, and  $\beta$ -thalassemia.<sup>44–46</sup> Consistent with most others' reports, HO-1 protein expression was enhanced in our model, which catalyzes heme degradation and facilitates the release of free iron. We speculate that the upregulated HO-1 in our erythrophagocytosis-induced EC model was mainly attributed to the regulation of the Nrf2 signaling pathway. Whether HO-1 is expressed in mature erythrocytes remains unclear, which needs to be investigated in our future study. Beside the iron metabolism, we also explored the key protein in amino acid metabolism pathway. SLC7A11 is a cystine/glutamate antiporter that mediates the efflux of cellular glutamate and the influx of cystine, which plays a role in ferroptosis due to regulation of the downstream synthesis of GPX4 and then catalyzed the reaction between GSH and lipid peroxides and prevent ferroptosis.<sup>47,48</sup> In our present cell model, erythrophagocytosis reduced the protein expression of SLC7A11 and GPX4, which may further facilitate the accumulation of lipid peroxide and contribute ferroptosis of EC. In an adenine-induced uremic rat model, we observed that RBCs showed specific binding and internalization by vECs in the kidney, and we considered that this could evoke serious damage to the vEC, and similarly to that observed *in vitro*, we noted erythrophagocytosis-induced mitochondrial damage. At the same time, we found that the contents of  $\text{Fe}^{3+}$ , the lipid peroxide MDA, and  $\text{H}_2\text{O}_2$  were increased in the kidney, while GSH, CAT, and SOD activities were decreased, all of which are characteristic indicators of ferroptosis.<sup>49</sup> Furthermore, the protein expression changes of FTN, FPN, HO-1, GPX4, SLC7A11, and TMEM16F in uremic rats were consistent with our *in vitro* experiments and could be reversed by blocking the phagocytic pathway or inhibition of ferroptosis. However, there is still a trend of increased thrombus size even with Fer-1 or DFO treatment in uremia condition, and we think that phosphatidylserine-exposed RBC/platelets/myeloid cells may involve in thrombogenesis in uremia, which has been demonstrated in our previous studies.<sup>10,11</sup> Combined, in the erythrophagocytosis model that mimics a uremic

environment and the uremic rat model, we revealed that increased heme upregulated the expression of HO-1, which promoted the release of free iron, thus increasing a variety of ROS and lipid peroxidation products through Fenton reaction and driving ferroptosis. Several ferroptosis-associated proteins including SLC7A11 and GPX4 also involved in this process. Further studies may need to elucidate the relationship of regulating mechanism between iron, GSH, and lipid metabolism in our model.

The relationship between EC dysfunction and subsequent thrombotic events is already well known in cardiovascular diseases, diabetes, and uremia.<sup>50,51</sup> Here, we are especially concerned about the significant involvement of the EC ferroptosis in the thrombotic complication of uremia. We found that the erythrophagocytosis led to the increase of phosphatidylserine externalization on the surface of ECs, which provided binding sites for clotting factors FXa and prothrombinase complexes, thus promoting the coagulation cascade reaction and subsequently leading to a dramatic increase in thrombin generation. By lactadherin inhibition assay, we further demonstrated that the increase in phosphatidylserine externalization after ferroptosis was the main reason for the enhancement of procoagulant activity in EC. TMEM16F is a  $\text{Ca}^{2+}$ -activated phospholipid scramblase located on the cell membrane, which moves phospholipids from the inner to the outer leaflet of the plasma membrane.<sup>25,40</sup> Recently, pieces of evidence have been provided that TMEM16F participates in cell apoptosis, ferroptosis, and pyroptosis.<sup>52–54</sup> We found increased TMEM16F expression in renal tissue of uremic rats and EC undergoing ferroptosis, which may explain the reason why phosphatidylserine externalization increased following ferroptosis in our model. In line with earlier reports describing that adenine-treated rats induce an increased thrombogenicity,<sup>55</sup> we found an adenine-induced uremic rat model exhibited enhanced thrombotic tendency by thromboelastography and IVC model. Additional pretreatment with Fer-1 to inhibit ferroptosis or annexin V to block the pathway of phagocytosis significantly decreased the hypercoagulability and ameliorated the flow restriction-induced venous thrombi in uremic rats, which demonstrated erythrophagocytosis-induced ferroptosis played a critical role in the high tendency of uremic thrombus formation, confirming our *in vitro* findings. Taken together, our present study not only indicated erythrophagocytosis-induced ferroptosis in EC, but also confirmed that TMEM16F-mediated phosphatidylserine exposure during the process of ferroptosis plays a major role in uremia-associated thrombosis. Additional studies are required to establish an *in vivo* experiment to inhibit the phagocytosis of macrophages, and to further determine the phagocytosis of RBCs and other peripheral blood cells or microparticles by ECs.

In conclusion, our findings suggest uremic RBC could trigger EC phagocytosis, ferroptosis, and thrombogenesis, which may be clinically relevant to the complication of uremia, such as anemia, infection, and thrombosis. Alternatively, inhibition of erythrophagocytosis or ferroptosis

could be a novel therapeutic strategy to alleviate the thromboembolic complication of uremia.

### What is known about this topic?

- Uremia might be at high risk of cardiovascular and thrombotic events; however, its mechanism is largely unknown.
- ECs as amateur phagocytes have phagocytic properties for lactadherin-opsonized RBC.
- The role of ferroptosis in the occurrence and development of thrombosis remains largely unclear.

### What does this paper add?

- Uremic RBC could trigger EC phagocytosis, ferroptosis, and thrombogenesis; TMEM16F-regulated PS exposure plays a key role in this process.
- Iron and amino acid metabolisms were involved in EP-triggered ferroptosis, which may be promising targets to prevent thrombosis of uremia.

### Authors' Contribution

Z.L. performed the experiments, analyzed the data, and edited the manuscript; Z.W., M.Y., Y.A., and L.W. performed the experiments and analyzed the data; M.X., Y.X., X.W., and T.L. contributed to the study design and commented on the manuscript; C.G. designed and conducted the research, analyzed, and interpreted the data, and wrote the manuscript.

### Funding

This work was supported by the National Natural Science Foundation of China (82070140 and 82270134), Marshal Initiative Funding (HMUMIF-22005), PhD Fund of Harbin Medical University-Daqing (XQBSQDJ201902), Natural Science Foundation of Heilongjiang Province (LH2020H0299), Heilongjiang Postdoctoral Science Foundation (LBHQ19127), Yu Weihai Foundation of Harbin Medical University (31021180167 and DQYWH201801), and Center of Diagnosis and Treatment of Disease in Cold Place, Harbin Medical University (CXZX-ZXKT01).

### Conflict of Interest

None declared.

### References

- Addi T, Dou L, Burtsey S. Tryptophan-derived uremic toxins and thrombosis in chronic kidney disease. *Toxins (Basel)* 2018;10(10):412
- Kelly DM, Rothwell PM. Prevention and treatment of stroke in patients with chronic kidney disease: an overview of evidence and current guidelines. *Kidney Int* 2020;97(02):266–278
- Schuett K, Savvaidis A, Maxeiner S, et al. Clot structure: a potent mortality risk factor in patients on hemodialysis. *J Am Soc Nephrol* 2017;28(05):1622–1630
- Basra SS, Tsai P, Lakkis NM. Safety and efficacy of antiplatelet and antithrombotic therapy in acute coronary syndrome patients with chronic kidney disease. *J Am Coll Cardiol* 2011;58(22):2263–2269
- Vance JE, Steenbergen R. Metabolism and functions of phosphatidylserine. *Prog Lipid Res* 2005;44(04):207–234
- Nagata S, Sakuragi T, Segawa K. Flippase and scramblase for phosphatidylserine exposure. *Curr Opin Immunol* 2020;62:31–38
- Zwaal RF, Schroit AJ. Pathophysiologic implications of membrane phospholipid asymmetry in blood cells. *Blood* 1997;89(04):1121–1132
- Shlomovitz I, Speir M, Gerlic M. Flipping the dogma - phosphatidylserine in non-apoptotic cell death. *Cell Commun Signal* 2019;17(01):139
- Li W. Eat-me signals: keys to molecular phagocyte biology and "appetite" control. *J Cell Physiol* 2012;227(04):1291–1297
- Gao C, Ji S, Dong W, et al. Indolic uremic solutes enhance procoagulant activity of red blood cells through phosphatidylserine exposure and microparticle release. *Toxins (Basel)* 2015;7(11):4390–4403
- Gao C, Xie R, Yu C, et al. Thrombotic role of blood and endothelial cells in uremia through phosphatidylserine exposure and microparticle release. *PLoS One* 2015;10(11):e0142835
- Slusarczyk P, Mleczko-Sanecka K. The multiple facets of iron recycling. *Genes (Basel)* 2021;12(09):1364
- Cambos M, Scorza T. Robust erythrophagocytosis leads to macrophage apoptosis via a hemin-mediated redox imbalance: role in hemolytic disorders. *J Leukoc Biol* 2011;89(01):159–171
- Youssef LA, Rebbaa A, Pampou S, et al. Increased erythrophagocytosis induces ferroptosis in red pulp macrophages in a mouse model of transfusion. *Blood* 2018;131(23):2581–2593
- Fens MH, Mastrobattista E, de Graaff AM, et al. Angiogenic endothelium shows lactadherin-dependent phagocytosis of aged erythrocytes and apoptotic cells. *Blood* 2008;111(09):4542–4550
- Fens MH, van Wijk R, Andringa G, et al. A role for activated endothelial cells in red blood cell clearance: implications for vasopathology. *Haematologica* 2012;97(04):500–508
- Dixon SJ, Lemberg KM, Lamprecht MR, et al. Ferroptosis: an iron-dependent form of nonapoptotic cell death. *Cell* 2012;149(05):1060–1072
- Jiang X, Stockwell BR, Conrad M. Ferroptosis: mechanisms, biology and role in disease. *Nat Rev Mol Cell Biol* 2021;22(04):266–282
- Ubellacker JM, Tasdogan A, Ramesh V, et al. Lymph protects metastasizing melanoma cells from ferroptosis. *Nature* 2020;585(7823):113–118
- Fang X, Wang H, Han D, et al. Ferroptosis as a target for protection against cardiomyopathy. *Proc Natl Acad Sci U S A* 2019;116(07):2672–2680
- Guo L, Zhang T, Wang F, et al. Targeted inhibition of Rev-erb- $\alpha/\beta$  limits ferroptosis to ameliorate folic acid-induced acute kidney injury. *Br J Pharmacol* 2021;178(02):328–345
- Tang LJ, Zhou YJ, Xiong XM, et al. Ubiquitin-specific protease 7 promotes ferroptosis via activation of the p53/TfR1 pathway in the rat hearts after ischemia/reperfusion. *Free Radic Biol Med* 2021;162:339–352
- Vanholder R, De Smet R, Glorieux G, et al; European Uremic Toxin Work Group (EUTox) Review on uremic toxins: classification, concentration, and interindividual variability. *Kidney Int* 2003;63(05):1934–1943
- Ji S, Dong W, Qi Y, et al. Phagocytosis by endothelial cells inhibits procoagulant activity of platelets of essential thrombocythemia in vitro. *J Thromb Haemost* 2020;18(01):222–233
- Yu H, Wang Z, Li Z, et al. Hyperuricemia enhances procoagulant activity of vascular endothelial cells through TMEM16F regulated phosphatidylserine exposure and microparticle release. *FASEB J* 2021;35(09):e21808

- 26 Kaur H, Fisher K, Othman M. Thromboelastography testing in mice following blood collection from facial vein and cardiac puncture. *Blood Coagul Fibrinolysis* 2019;30(07):366–369
- 27 Yokozawa T, Zheng PD, Oura H, Koizumi F. Animal model of adenine-induced chronic renal failure in rats. *Nephron J* 1986;44(03):230–234
- 28 Ravid JD, Kamel MH, Chitalia VC. Uraemic solutes as therapeutic targets in CKD-associated cardiovascular disease. *Nat Rev Nephrol* 2021;17(06):402–416
- 29 Ganz T. Macrophages and iron metabolism. *Microbiol Spectr* 2016;4(05):10
- 30 Nagata S, Hanayama R, Kawane K. Autoimmunity and the clearance of dead cells. *Cell* 2010;140(05):619–630
- 31 Visan I. Amateur phagocytes. *Nat Immunol* 2019;20(03):245
- 32 Sihombing MAEM, Safitri M, Zhou T, et al. Unexpected role of nonimmune cells: amateur phagocytes. *DNA Cell Biol* 2021;40(02):157–171
- 33 de Back DZ, Kostova EB, van Kraaij M, van den Berg TK, van Bruggen R. Of macrophages and red blood cells; a complex love story. *Front Physiol* 2014;5:9
- 34 Bonomini M, Siroli V, Reale M, Arduini A. Involvement of phosphatidylserine exposure in the recognition and phagocytosis of uremic erythrocytes. *Am J Kidney Dis* 2001;37(04):807–814
- 35 Diaz-Ricart M, Torramade-Moix S, Pascual G, et al. Endothelial damage, inflammation and immunity in chronic kidney disease. *Toxins (Basel)* 2020;12(06):361
- 36 Das S, Zhang E, Senapati P, et al. A novel angiotensin II-induced long noncoding RNA giver regulates oxidative stress, inflammation, and proliferation in vascular smooth muscle cells. *Circ Res* 2018;123(12):1298–1312
- 37 Gao C, Xie R, Li W, et al. Endothelial cell phagocytosis of senescent neutrophils decreases procoagulant activity. *Thromb Haemost* 2013;109(06):1079–1090
- 38 Xie R, Gao C, Li W, et al. Phagocytosis by macrophages and endothelial cells inhibits procoagulant and fibrinolytic activity of acute promyelocytic leukemia cells. *Blood* 2012;119(10):2325–2334
- 39 Catan A, Turpin C, Diotel N, et al. Aging and glycation promote erythrocyte phagocytosis by human endothelial cells: potential impact in atherothrombosis under diabetic conditions. *Atherosclerosis* 2019;291:87–98
- 40 Yan M, Xu M, Li Z, et al. TMEM16F mediated phosphatidylserine exposure and microparticle release on erythrocyte contribute to hypercoagulable state in hyperuricemia. *Blood Cells Mol Dis* 2022;96:102666
- 41 Li J, Cao F, Yin HL, et al. Ferroptosis: past, present and future. *Cell Death Dis* 2020;11(02):88
- 42 Virág L, Jaén RI, Regdon Z, Boscá L, Prieto P. Self-defense of macrophages against oxidative injury: fighting for their own survival. *Redox Biol* 2019;26:101261
- 43 Fernández-Mendivil C, Luengo E, Trigo-Alonso P, García-Magro N, Negro P, López MG. Protective role of microglial HO-1 blockade in aging: implication of iron metabolism. *Redox Biol* 2021;38:101789
- 44 Menon AV, Liu J, Tsai HP, et al. Excess heme upregulates heme oxygenase 1 and promotes cardiac ferroptosis in mice with sickle cell disease. *Blood* 2022;139(06):936–941
- 45 Wang H, An P, Xie E, et al. Characterization of ferroptosis in murine models of hemochromatosis. *Hepatology* 2017;66(02):449–465
- 46 Garcia-Santos D, Hamdi A, Saxova Z, et al. Inhibition of heme oxygenase ameliorates anemia and reduces iron overload in a  $\beta$ -thalassemia mouse model. *Blood* 2018;131(02):236–246
- 47 Lang X, Green MD, Wang W, et al. Radiotherapy and immunotherapy promote tumoral lipid oxidation and ferroptosis via synergistic repression of SLC7A11. *Cancer Discov* 2019;9(12):1673–1685
- 48 Imai H, Matsuoka M, Kumagai T, Sakamoto T, Koumura T. Lipid peroxidation-dependent cell death regulated by GPX4 and ferroptosis. *Curr Top Microbiol Immunol* 2017;403:143–170
- 49 Dong H, Qiang Z, Chai D, et al. Nrf2 inhibits ferroptosis and protects against acute lung injury due to intestinal ischemia reperfusion via regulating SLC7A11 and HO-1. *Aging (Albany NY)* 2020;12(13):12943–12959
- 50 Babik B, Peták F, Agócs S, et al. [Diabetes mellitus: endothelial dysfunction and changes in hemostasis]. *Orv Hetil* 2018;159(33):1335–1345
- 51 Torramade-Moix S, Palomo M, Vera M, et al. Apixaban down-regulates endothelial inflammatory and prothrombotic phenotype in an in vitro model of endothelial dysfunction in uremia. *Cardiovasc Drugs Ther* 2021;35(03):521–532
- 52 Liu G, Liu G, Chen H, et al. Involvement of  $\text{Ca}^{2+}$  activated  $\text{Cl}^{-}$  channel Ano6 in platelet activation and apoptosis. *Cell Physiol Biochem* 2015;37(05):1934–1944
- 53 Ousingawatt J, Wanitchakool P, Schreiber R, Kunzelmann K. Contribution of TMEM16F to pyroptotic cell death. *Cell Death Dis* 2018;9(03):300
- 54 Ousingawatt J, Schreiber R, Kunzelmann K. TMEM16F/Anoctamin 6 in ferroptotic cell death. *Cancers (Basel)* 2019;11(05):625
- 55 Nemmar A, Al-Salam S, Beegam S, et al. Cardiac inflammation, oxidative stress, Nrf2 expression, and coagulation events in mice with experimental chronic kidney disease. *Oxid Med Cell Longev* 2021;2021:8845607